OPEN ACCESS

Base-Driven Ring-Opening Reactions of Vinylene Carbonate

Journal of The Electrochemical Society, 2024 **171** 050506

Base-Driven Ring-Opening Reactions of Vinylene Carbonate

Neeha Gogoi,[z] Robin Lundström, Guiomar Hernández, and Erik J. Berg[z]

Department of Chemistry, Ångström Laboratory, Uppsala University, SE-751 21 Uppsala, Sweden

Vinylene carbonate (VC) is the most commonly applied performance-enhancing electrolyte additives in Li-ion batteries to date. Despite numerous studies, there is a lack of consensus regarding the various reaction pathways of VC and their implications. VC has primarily been observed to either polymerize forming poly(vinylene carbonate) (poly(VC)) or decompose releasing major amounts of CO_2, two seemingly contradictory processes. Herein, we present evidence of additional reaction pathways of VC highlighting its role as a H_2O scavenging agent. In contrast to the typical electrolyte solvent ethylene carbonate, VC reacts much more rapidly with water impurities, especially when in contact with hydroxides, forming products less likely to influence cell performance. Efficient removal of water and hydroxides is essential to preserve the stability of Li-ion electrolyte solvent and salt, hence guaranteeing a long lifetime of the battery. Model studies pinpointing reaction pathways of electrolytes and additives, as presented herein, are critical not only to improve modern Li-ion cells but also to establish design principles for future battery chemistries.

 [DOI: 10.1149/1945-7111/ad430e]

Manuscript submitted February 18, 2024; revised manuscript received March 27, 2024. Published May 7, 2024.

Supplementary material for this article is available online

Electrolyte additives are ubiquitous in batteries. The most common additive in modern Li-ion batteries is vinylene carbonate (VC), largely due to its unique ability to efficiently stabilize the negative electrode. Following its incorporation in Li-ion batteries since the early 2000s, several reaction pathways of VC have been proposed. VC contains a C=C double bond which is known to trigger polymerization during reductive decomposition to form oligomers and insoluble polymers as illustrated in Rxn 1–7 below. Several experimental[1–3] and computational studies[4,5] have shown that after the initial reduction of VC molecule (Rxn 1), a radical anion (containing an unpaired electron) is formed following the ring-opening, which acts as an initiator for a radical polymerization on C=C (homolysis) unit. The resulting polymer consists of repeating units of ethylene carbonate (EC), often referred to as poly(VC).[5] VC has also been suggested to undergo polymerization through its carbonate group, thus forming polycarbonate and/or polyethylene substituted with $–OCO_2Li$ groups (Rxn 2).[6] The poly(VC) has subsequently been reported to undergo a 2-electron reduction to produce Li_2CO_3 and polyacetylene (Rxn 3).[1,3,4,7]

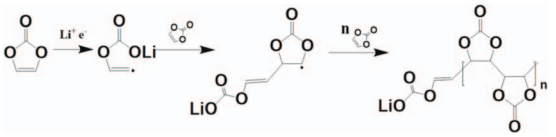

[1]

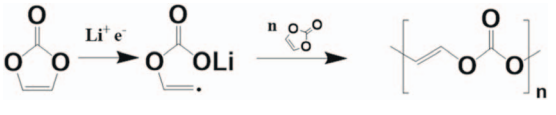

[2]

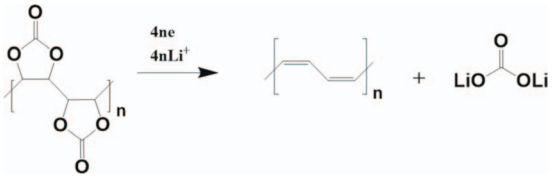

[3]

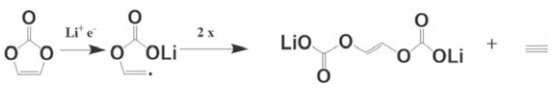

[4]

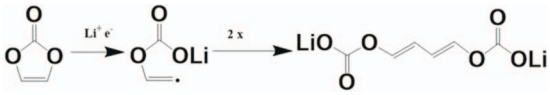

[5]

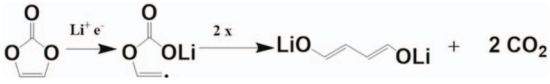

[6]

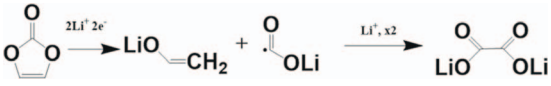

[7]

Alternatively, the VC radical anion formed following VC ring-opening has also been proposed to rather generate lithium vinylene dicarbonate ($(=CH–OCO_2Li)_2$ (Rxn 4),[3] lithium divinylene dicarbonate ($(=CH–CH–OCO_2Li)_2$ (Rxn 5)[3] and/or lithium divinylene dialkoxide (Rxn 6)[1] as a result of dimerization reactions. These dimers can potentially aggregate further, forming oligomers consisting of 3, 4, or more units via O···Li···O interactions.[8] Additionally, VC is suggested to form inorganic lithium salts, such as Li-oxalate or Li_2CO_3 (Rxn 7). Because of their low electrolyte solubility, some of these products are believed to precipitate to form a Li^+-conducting layer on the surface of the negative Li-ion electrode, namely a solid electrolyte interphase (SEI), which in turn prevents further electrolyte degradation and thereby guarantees stable operation of the negative electrode. An essential feature is that VC reacts at higher electrode potentials before its saturated counterparts, i.e., the cyclic and linear electrolyte solvents, e.g., EC and diethyl carbonate (DEC). Depending on the choice of the methodology and amount of VC present in the electrolyte formulation, proposed VC reduction potentials vary from 0.57–1.80 V vs Li/Li^+ range.[1,3,9–13] In a theoretical study by Balbuena and team,[4] they calculated the VC reduction potential to be ∼0.4 V less negative than EC, which would correspond to ∼1.2 V vs Li^+/Li.

There is also a general agreement that VC acts as a source of CO_2, a well-known beneficial component for SEI formation and performance of the battery.[3,13] CO_2 evolution is seemingly independent from poly(VC) formation, as the latter contains intact carbonate moieties, and is instead likely a result of base-driven ring-opening of VC. A number of Lewis bases may form during the SEI formation process, of which especially OH^-, a typical reduction product of H_2O impurities, is well-known to ring-open the cyclic carbonates and initiate an autocatalytic reaction that ultimately produces glycols

[z]E-mail: neeha.gogoi@kemi.uu.se; erik.berg@kemi.uu.se

and CO_2.[14] Although many components of the cell are prone to hydrolysis, we hypothesize that VC is particularly susceptible to a nucleophilic attack and ring-opening, thus explaining the previously observed strong evolution of CO_2.

The aim of the current study is therefore to investigate the base-driven degradation of VC when exposed to Lewis bases. Drawing parallels of this reaction to a practical cell, during first negative polarization, it is expected that the oxygen containing surface groups on the negative electrode surface or water residues present (O^-, O^{2-}, OH^-) in cell induces a nucleophilic attack on the VC, which in turn ring-opens and kickstarts a series of decomposition reactions. Thus, the VC ring-opening is expected to essentially be an electrochemically activated and chemically propagated reaction process. We study herein these chemical reactions and identify the species formed upon ring-opening and successive decomposition of VC that accompanies the evolution of gaseous CO_2. We suspect more functionality of VC and hence will investigate if the ring-opened reaction products of VC is further responsible to subsequently scavenge residual H_2O from the electrolyte.

Experimental

Materials.—DME (99.9% purity, Honeywell) and VC (Sigma-Aldrich, chemical purity >99%) were used as received from suppliers. TBAOH·30H_2O (tetrabutylammonium hydroxide-30 hydrate, chemical purity >99%, Sigma-Aldrich) was added as a chemical source of OH^- with H_2O.

Electrochemistry and online gas evolution.— *Online electrochemical mass spectrometry (OEMS).*—Cyclic voltammetry was performed on a custom-made OEMS cell containing glassy carbon as working electrode in 1 M $LiPF_6$ in EC:DEC (1:1 v/v) (LP40). The potential was swept from OCP down to 0.05 V vs Li^+/Li and back to 1.7 V vs Li^+/Li with a scan rate of 0.1 mV s^{-1}. The glassy carbon working electrodes (∅ 15 mm) were prepared by coating a stainless-steel mesh (212/90 μm, Bopp AG, Switzerland) with glassy carbon powder (Sigma-Aldrich, spherical powder, 2–12 μm, 99.95% trace metals basis, A_{BET} = 1.8 m^2 g^{-1}) by slurry deposition at room temperature. To avoid gas evolution from the counter electrode, $LiFePO_4$ electrodes (∅ 15 mm, Custom cells, 1 mAh cm^{-2}, Germany) were used which were delithiated to 3.43 V vs Li^+/Li before assembly. The OEMS cell set-up and the data treatment procedure has been described in a previous publication.[15]

Injection cell-coupled mass spectrometer.—As the hydrolysis rates of the carbonates in question shall be determined as a function of temperature, a testing procedure utilizing distinct temperature increments is implemented. A dedicated injection cell was used, where a syringe was connected to a gas tight vial that could be connected to the OEMS set-up. DME mixed with carbonate (EC and VC separately) was taken in the syringe and DME mixed with TBAOH.30H_2O was taken at the bottom of the vial. The amounts of the carbonates and the TBAOH.30H_2O were adjusted such that the overall concentrations of 1 mol L^{-1} and 0.06 mol L^{-1} respectively, are achieved upon mixing. After connecting the injection cell to the mass spectrometer, the cell temperature is first held at 30 °C for 2 h such that a baseline for ion currents H_2-2, H_2O-18, methane-15,16, ethane- 26, 28, 30, methanol-31, ethanol- 31, 45, 46, O_2-32, Ar-36, CO_2-44, DME-45, 29 were recorded. The time between each sampling point was set to 3 min. Once a stable background is achieved, reactants from the syringe were mixed with the reactants in the vial and periodic sampling was done as stated previously. Subsequently, the temperature was set to 40, 50 and 60 °C and held for ∼1 h at each temperature step. As references, baseline measurements were performed where DME was injected into H_2O mixed with DME, DME was injected into TBAOH.30H_2O mixed with DME and carbonates mixed with DME was injected into H_2O mixed with DME.

Nuclear magnetic resonance (NMR).—The degradation products formed from thermally aged solution of TBAOH.30H_2O+VC mixture was analyzed with solution NMR spectroscopy. For that, TBAOH.30H_2O was mixed in VC in the same proportion and in the same condition as in the gas evolution reaction as mentioned above, but now deuterated DMSO was used as the background instead of DME. All spectra were recorded at room temperature, and anhydrous DMSO-d_6 was used as the internal standard for ^{1}H (2.46 ppm) and ^{13}C NMR (39.9 ppm). The reason for replacing DME with DMSO-d_6 was to have a more resolved and intensified signals from the reaction products without the interference of DME signals. For comparison, NMR analysis of the reaction products analyzed for TBAOH.30H_2O+VC mixture where DME was the background solvent are described in supplementary information.

All NMR spectra were obtained using an NMR spectrometer (JEOL ECZ 400 S) operating at 400 MHz for the ^{1}H nucleus and 100 MHz for the ^{13}C nucleus. The conditions for the ^{1}H-NMR were 45° pulse angle, 8 s delay between pluses, 20.0 kHz spectral width, and 64 scans. The conditions for the ^{13}C NMR were a 45° pulse angle, 1.8 s delay between pluses, 27 kHz spectral width, and 1024 scans. The Heteronuclear Multiple Bond Correlation (HMBC) and Heteronuclear Single Quantum Coherence (HSQC) spectra were acquired using 16 scans for f1 and f2 of 512 t1 and 256 t1 increments.

Karl Fischer titration (KFT).—To determine the amount of water consumed during VC decomposition, a series of electrolyte mixtures were prepared and tested with coulometric Karl Fischer titrator (Mettler-Toledo). DME was taken as the background solvent. The first series of electrolyte mixture was prepared by deliberately contaminating the DME with 667 ppm of H_2O. To that mixture, VC added such that overall DME:VC = 99:1 v/v ratio is obtained. The second series of electrolyte was prepared by adding TBAOH.30H_2O in DME. The concentrations of TBAOH.30H_2O were adjusted to achieve the same H_2O concentrations in the electrolyte as in the H_2O-containing electrolytes. To the DME+ TBAOH.H_2O mixture, VC was added such that overall DME:VC is 99:1 v/v. Similar procedure was followed to prepare an electrolyte solution where VC was replaced with EC. We recorded how much H_2O (in ppm) is present at 4 h, 24 h and 6 d after mixing and subtracted H_2O recorded at the time of mixing from them.

Fourier transform infrared spectroscopy (FTIR).—FTIR measurements of samples were obtained on a Bruker spectrometer. The spectra were acquired in the attenuated total reflection with 4 cm^{-1} resolution and 64 total scans. FTIR calibration curves of VC in DME and TBAOH.H_2O in DME were prepared. Intensity (a.u.) of VC (–CH=CH–) monomer centred at 3161 cm^{-1} and water (–OH) bands centred at 1639 cm^{-1} and 3393 cm^{-1} are considered for their quantifications. Fresh solution of VC:TBAOH.30H_2O in different composition such that the molar ratio of VC:H_2O are 3.84:7.66, 3.84:6.38, 3.84:4.99, 3.84:3:48 were obtained in DME background solvent. 100 uL of the prepared solution was added into the ATR crystal inside the GB and covered with a metallic pate with an O-ring such that the sample is airtight. FTIR spectra were recorded in every 3 min. The hydrolysis reaction of VC was quantified by FTIR; the vibration of VC and water were determined and the changes in the peak intensities were monitored at RT during the reaction time. Baseline subtraction was done to remove any background signals.

Results and Discussion

Operando gas evolution during reductive decomposition of VC.—Figure 1 shows the (a) cyclic voltammogram along with (b) H_2, (c) CO_2 and (d) C_2H_4 gas evolution profiles during reduction of a typical organic carbonate-based Li-ion electrolyte (1 M $LiPF_6$ in 1:1 EC:DEC, v/v) without (black) and with 1 v% VC (red) added. A porous glassy carbon electrode was applied instead of graphite to monitor the (electro-/)chemical surface reactions to avoid the influence of solvent co-intercalation with Li^+ into graphite. The current is largely dominated by de-/adsorption of Li^+ in the

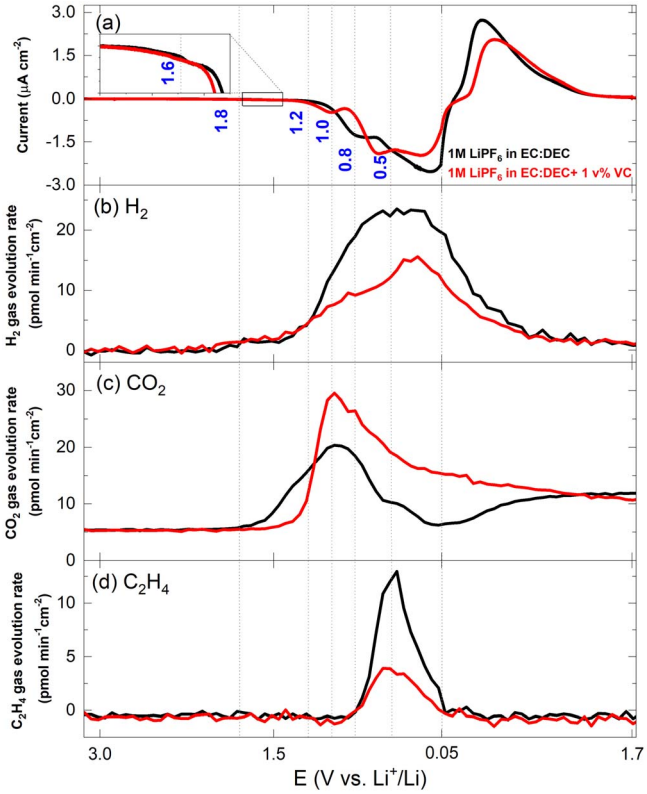

Figure 1. (a) Cyclic voltammogram from GC|LP40| LFP OEMS cell with (red) and without VC (black) cycled with CV at 0.1 mV s^{-1} rate, with a zoom-in on ~1.6 V electrochemical profiles. Simultaneous (b) H_2, (c) CO_2 and (d) C_2H_4 gas evolution rates (pmol min^{-1} cm^{-2}) as measured.

nanoscale surface crevices of glassy carbon.[16] Faradaic decomposition reactions are however discerned. In absence of VC, a minor current peak associated with H_2O reduction is observed <1.6 V (see inset) followed by EC and CO_2 reduction <1.0 V. On the other hand, for the VC containing electrolyte, no clear indication of H_2O reduction is observed from the current, even though H_2 is observed to set in at the same potentials. H_2 is generally evolved from the reduction of trace water present in the cell. The amount of H_2 evolved when VC is added is clearly less and points to the fact that VC interacts with water in the Li-ion cell. Below 1.2 V, a new current peak is observed when VC is present and likely related to Li-formate formation

$$Li^+ + CO_2 + H^+ + 2e^- \rightarrow HCO_2Li \quad [8]$$

involving consumption of proton, which also contributes to the lower H_2 evolution rate. Again <1.0 V, direct CO_2 reduction kicks in hence explaining the rapidly diminishing CO_2 evolution rate. The VC-derived SEI layer suppresses EC reduction judging from lower evolution of C_2H_4 and is more resistive as less reversible current is observed.[10] Although CO_2 sets in a bit later when VC is present, the CO_2 gas evolution rate rises steeply at 1.4 V and the amount of CO_2 evolved is higher than the cell without VC. If we consider one mole of VC converts into one mole of CO_2, and that all the CO_2 observed for VC-containing electrolyte is solely from VC decomposition, then ~10% of the added VC in the electrolyte would be used up. The CO_2 evolution observed for VC which continues after the end of the reductive CV scan likely belongs to a chemical chain reaction which eliminates CO_2.[7] Its worth noting that no indication of acetylene evolution was found and the extent of Rxn 4 is likely insignificant. In any case, we learn from the experiment above that both EC and VC are prone to ring-opening and CO_2 release, although the rate of the reactions are seemingly faster for VC. These possible hydrochemical degradation processes have been overlooked in many earlier studies because VC degradation processes often show up at the H_2O reduction potential and are therefore assumed to be purely electrochemical. However, our gas data hints that the chemical propagation reactions initiated by H_2O reduction and OH^- formation are prevalent. In order to further elucidate these hydrochemical degradation processes, we performed an injection cell-coupled mass spectrometry experiment where we exposed both EC and VC directly to water and hydroxide.

CO_2 gas evolution rate monitoring and effect of temperature on the evolution.—Figure 2 shows the CO_2 evolution vs time when (a) EC and (b) VC are injected into a solution of H_2O dissolved in DME in absence (green) and presence (blue) of TBAOH. The reason for choosing TBAOH as the hydroxide containing salt instead of LiOH (which otherwise would have been more relevant for a LIB environment) is due to the higher solubility of TBAOH in DME. DME was here used as a background solvent to compare the ring-opening of EC and VC under similar conditions because of its superior chemical stability towards Lewis bases,[17] thus avoiding the influence of other linear and cyclic carbonate (e.g., EC and/or DEC). Figure 2 (upper panel) shows the temperature set point in red dashed line. Temperature was stepwise increased during the experiment to accelerate the chemical reactions. The grey area shows the time when the baseline measurement was being performed.

Clearly, the CO_2 evolution traces for the two formulations suggest fundamentally different reaction kinetics for the hydrolysis of EC and VC in the presence of OH^- ions (blue trendline in Figs. 2a and 2b, respectively). Throughout the complete series of measurements, no gases other than CO_2 were detected. There is virtually no CO_2 evolution for EC and VC when exposed to only water as can be seen with the green trendline in Figs. 2a and 2b. Hence the evolution of CO_2 from the carbonate decomposition can be credited to OH^-. Based on the data in Fig. 2a, the apparent activation energy of EC hydrolysis driven by OH^- is found to be ~64 KJ mol^{-1} from the Arrhenius plot (Fig. S1), which agrees with the previous report by Metzger et al.[14] However, compared to EC, the alkaline hydrolysis of VC proceeds much faster and to a larger extent, which makes an estimate of same activation energies for VC impossible with this method. In any case, since the CO_2 evolution rate is two orders of magnitude higher for VC compared to EC, the activation barrier of VC hydrolysis at RT is much lower than for EC. Furthermore, the released CO_2 likely reacts with nearby OH^- to form carbonates and bicarbonates (through Rxn 9 and 10) as evidence by FTIR below

$$CO_2 + OH^- \rightarrow CO_3^{2-} + H^+ \quad [9]$$

$$CO_2 + OH^- \rightarrow HCO_3^- \quad [10]$$

These carbonates, once formed, are more stable towards the electrolyte than OH^-. In other words, CO_2 deactivates the OH^-, which in turn could also explain why we do not see an increase in the CO_2 evolution rate even if the temperature is ramped up to higher magnitude. For EC, the CO_2 evolves at a slower rate and hence, the deactivation of the hydroxide takes longer time. As a result, there is temperature dependent growth of CO_2 evolution. The immediate formation of high local concentration of CO_2 during SEI formation is likely a beneficial effect of VC.

We estimated the overall conversion of EC and VC from the total amount of evolved CO_2 at the end of each temperature step for all of the investigated electrolytes shown in Table I.

The consumption of VC and EC is calculated from the CO_2 release measured by MS, under the assumption that 1 mol CO_2 originates from the decomposition of 1 mol VC and EC respectively. Clearly, there is no one-to-one relation between CO_2 evolution and VC present in the electrolyte. There is a lot of VC molecules in the solution left unreacted. This observation can be correlated to the results of the OEMS experiment in Fig. 1, where 90% of VC is found to remain unreacted.

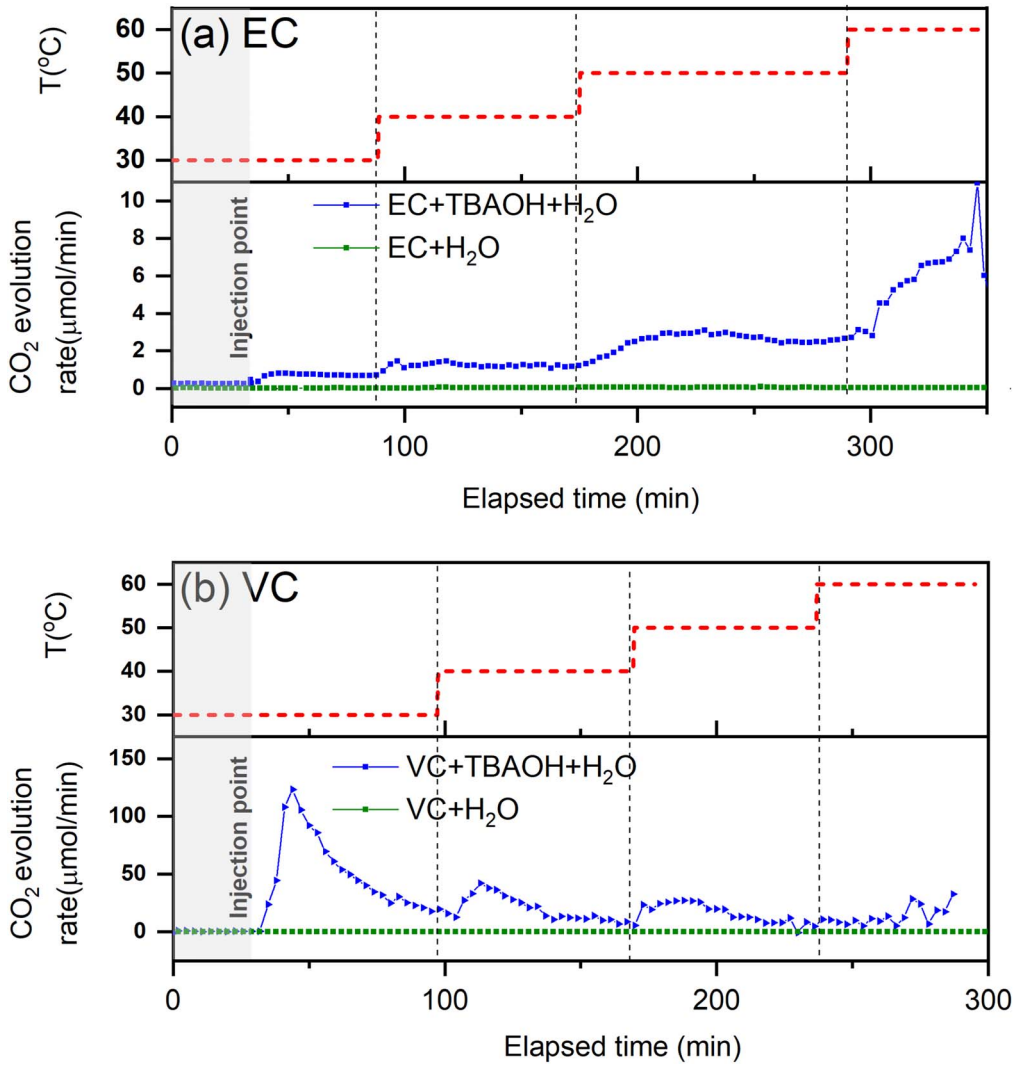

Figure 2. Red dashed line represents the temperature set point (upper panel) vs time during (a) EC and (b) VC hydrochemical reaction, in presence (blue) and absence (green) of TBAOH in DME background solvent (lower panel). The evolution rate of CO_2 in the head space of the injection vial is represented in μmol/min.

Table I. Overview of evolved amounts of CO_2 in mols, as quantified by online-MS, at different temperature steps.

	CO_2 evolved (mols)			
Set temperature (° C)	Initial [EC] = 1 mol L^{-1} Initial [TBAOH.30H_2O] = 0.06 mol L^{-1}	Initial [VC] = 1 mol L^{-1} Initial [TBAOH.30H_2O] = 0.06 mol L^{-1}	Initial [VC] = 1 mol L^{-1} Initial [TBAOH.30H_2O] = 0.03 mol L^{-1}	Initial [VC] = 0.5 mol L^{-1} Initial [TBAOH.30H_2O] = 0.06 mol L^{-1}
30	3.96E-06	3.65E-04	3.65E-04	2.317E-04
40	1.00E-05	1.24E-04	1.190E-04	6.058E-05
50	2.47E-05	1.066E-04	9.164E-05	3.04E-05
60	4.97E-05	2.87E-05	3.896E-05	3.234E-05

Another reason for not observing the stoichiometric relation between CO_2 released and VC present could be that, in addition to the decarboxylation reaction, VC is taking part in some other reaction where carbonate unit is still intact, a discussion about which will be done below.

The effect of varying the TBAOH.30H_2O and VC concentrations on the chemical reaction was studied. The amount of CO_2 detected during the reaction is listed in Table I. It is obvious that lowering the amount of TBAOH.30H_2O by half does not have any effect on the amount of CO_2 evolved. But lowering the amount of VC in the sample mixture lowers the amount of CO_2 evolved. This suggests that the quantity of VC directly influences the extent of the CO_2 evolution reaction. Higher concentrations of VC lead to stronger CO_2 evolution. VC is therefore foreseen to react with OH^- generating a reactive species which subsequently reacts with additional VC molecules, resulting in more CO_2 evolution (through Rxn 11 and 12).

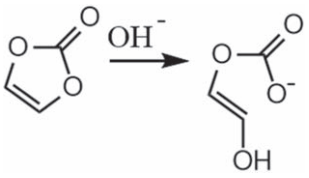

[11]

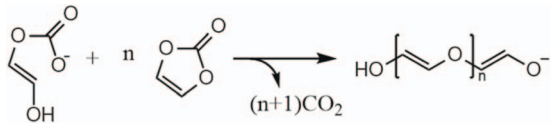

[12]

Likely, the CO_2 evolution reaction is governed by the propagation (mass transport) of ring-opened VC to react with neighbouring intact VC. The higher the VC concentration, the shorter the distance a ring-opened VC has to travel to meet another VC, which in turn trigger more VC decomposition evolving CO_2. This finding is in line with study made in the Dahn research group where they report that the amount of CO_2 evolved scales with the amount of VC present.[18] Conversely, when there is an increased concentration of TBAOH.30H_2O, more of that reactive specie are formed which undergo an alternative reaction, possibly by combining with similar species without CO_2 evolution. The VC hydrolyzed solution was observed to degrade during storage as indicated by increasingly dark coloration finally leading to an insoluble dark viscous gel-like product precipitating at the bottom of the vial (Fig. S2). On the other hand, EC hydrolyzed solution was observed to be color-free without precipitation. This product was analysed with NMR, in an attempt to identify the solubilised reaction products and discussed below.

Hydrolysis reaction rates of carbonates.—Considering that H_2 primarily stems from water reduction and the consistently lower amount of H_2 evolving in OEMS cells containing VC, Fig. 1, one can imagine either of two cases: (i) the SEI formed due to VC reduction passivates the negative electrode surface before H_2O reduction potential is reached. Alternatively, (ii) VC itself or one of its products scavenges/consumes H_2O. Infact, Gasteiger and team credited the SEI layer formed by pre-cycling the graphite electrode in 2 v% VC containing electrolyte to reduce the H_2 evolution in water-containing electrolyte by a factor of 7.5 compared to a pristine graphite electrode.[2]

Thus, in order to test the hypothesis that VC is responsible for water scavenging, we employed KFT to quantify the amount of water being consumed.

KFT was performed on a series of electrolytes containing VC that was deliberately contaminated with 667 ppm H_2O with and without TBAOH. For comparison, same experiment was also conducted for series of samples containing EC. Figure 3 summarizes the water consumed in those different electrolyte formulations along with their blank standards. The bar going down represents the consumption of H_2O.

First, the solutions with DME+VC/EC and DME+H_2O display very minor changes in water concentration over the course of the experiments (6 days). Furthermore, the amount of H_2O in the solution where only VC was present remains the same for the first 24 h. A slight decrease in the H_2O content was only noticeable when stored for over 6 days. However, when OH^- is present in the solution, VC is able to scavenge H_2O at a much faster rate. About 100 ppm of H_2O was consumed in 4 h and more than 200 ppm of H_2O was consumed after 24 h of storage. Interestingly, no further H_2O consumption was noted thereafter. EC also shows a trend similar as VC but to a much lesser extent. A significant decrease of H_2O content was only observed when DME+EC+TBAOH.30H_2O was stored for 6 days. This points in the direction that once VC is ring-opened by the hydroxide, it is able to scavenge H_2O. VC also consumes H_2O on its own but the rate is slower than when hydroxide is present. The role played by ring-opened VC as initiator of the water consumption process is hence evidenced.

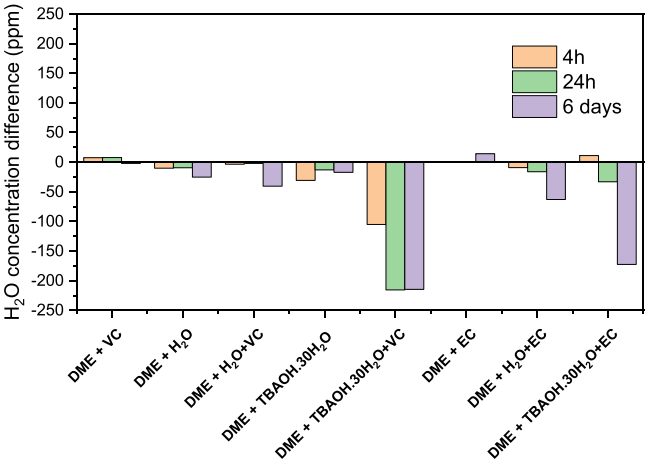

Figure 3. Amount of water consumed by VC and EC in presence and absence of OH^- at different reaction times recorded at RT. The amount of water present in the background solvent were also measured over the same period of time: 4 h, 24 h and 6 days after mixing and subtracted H_2O recorded at the time of mixing from them. The bar going down represents the consumption of H_2O.

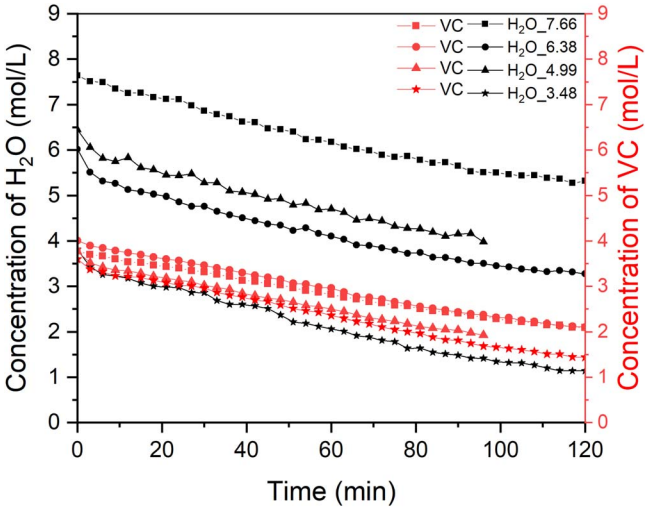

Figure 4. The change in the concentrations of VC and H_2O as quantified from the FTIR spectra during the hydrolysis reaction. The starting concentrations of VC is taken to be 3.84 mol L^{-1} while the concentrations of hydroxide and water were varied.

The KFT data is quite telling of how fast the reaction happens. In order to further elucidate the mechanism behind, the rate of reaction was followed with different concentrations of H_2O (7.66 (OH^- 0.25 mol L^{-1}), 6.38 (OH^- 0.21 mol L^{-1}), 4.99 (OH^- 0.17 mol L^{-1}), 3.48 (OH^- 0.12 mol L^{-1}) mol L^{-1}) by measuring the amount of VC and H_2O consumed as a function of time by FTIR. Figure 4 shows the change in the concentrations of VC (starting from 3.84 mol L^{-1}) and H_2O as quantified from the FTIR spectra during the hydrolysis reaction.

Surprisingly, the ratio of the consumption rate of VC to H_2O is consistently 1:1 across various compositions. Regardless of the amount of TBAOH.30H_2O added to the solution, the consumption rate of VC remains constant. This observation confirms the findings of the injection cell experiment where we recorded same amount of CO_2 evolution in VC+TBAOH.30H_2O reaction mixtures irrespective of the TBAOH.H_2O concentration.

NMR characterisation of the decomposition products.—The solubilised reaction products were analysed with NMR

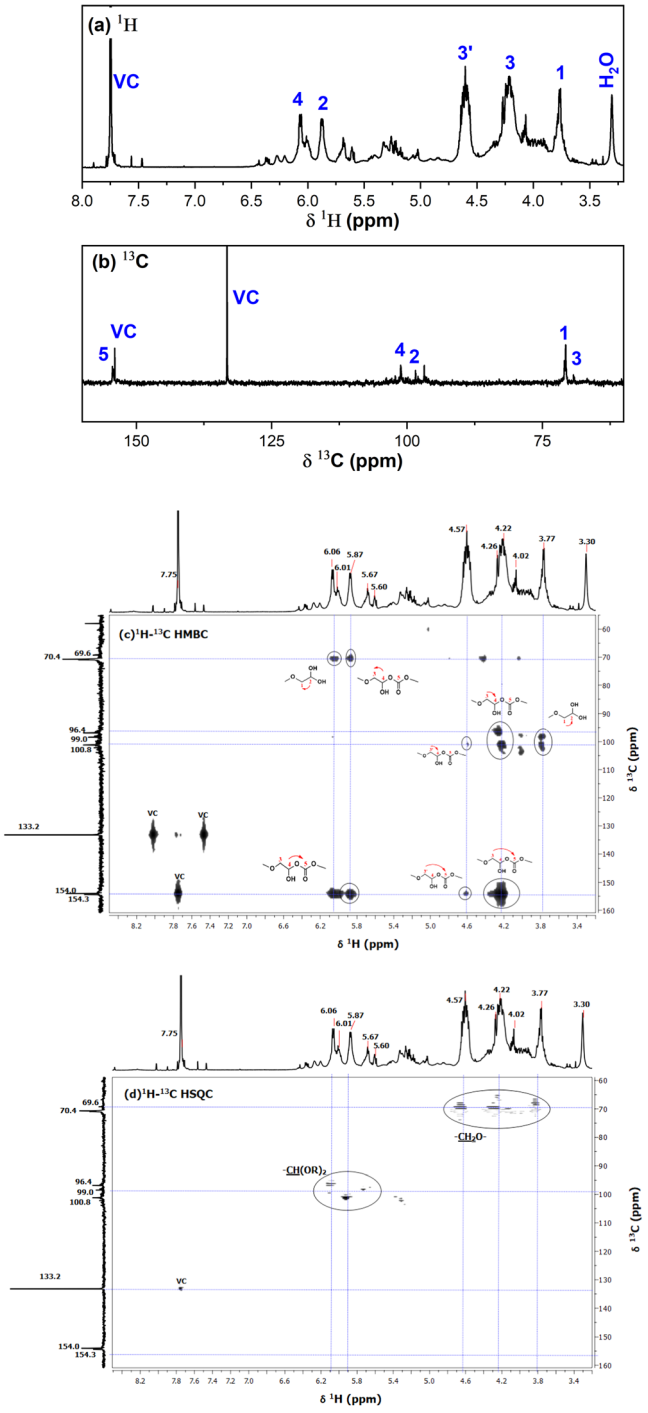

Figure 5. (a)–(d) ^{1}H, ^{13}C, 2D ^{1}H-^{13}C HMBC and ^{1}H-^{13}C HSQC NMR spectra of the solubilized reaction product. The numbers in blue in (a) and (b) are assigned to the carbons and protons that will be used for their assignment in Table II.

spectroscopy. For that the precipitate was recovered from the injection experiment and then dissolved in DMSO-d_6. The residual DME solvent cast strong signals in ^{1}H NMR spectrum overlapping with signals from the decomposition reaction product making the identification of the products extremely challenging (Fig. S3). However, the DME solutions containing VC, H_2O, and TBAOH were also analysed with gas chromatography coupled with mass spectrometry (GC-MS), but no products other than CO_2 were observed. The reaction products of VC hydrolysis are likely insoluble in DME and precipitate out of the solution. Therefore, DME was replaced with DMSO-d_6, which offers better solubility of the reaction products. VC and TBAOH.30H_2O was mixed in the same proportion as that used in the injection experiment. Figures 5a and 5b represents the ^{1}H and ^{13}C spectra recorded for the aforementioned mixture. An overview of the assignments of the observed chemical shifts is given in Table II. The assignments of the NMR signals are decided by a combination of complementary and detailed two-dimensional NMR experiments (^{1}H-^{13}C HMBC and HSQC in Figs. 5c and 5d).

The ^{1}H NMR spectrum (Fig. 5a) shows a singlet at 7.78 ppm for the protons in the VC. The ^{1}H NMR spectrum over the full shift range (10−0 ppm) is presented in Fig. S3 (along with the spectra for the individual components). The carbon peaks for –CH=CH– and C=O in ^{13}C NMR spectrum (Fig. 5b) for VC is at 133.2 and 154 ppm respectively. It is clearly observed that the spectra for the reaction product contain several new and weaker signals in both ^{1}H and ^{13}C-NMR spectra, suggesting to a broader spread of hydrolyzed VC fragments. Two dominating species have been identified and their structures are illustrated in Scheme 1 as Structure 1 and 2 together with our proposed reaction schemes to form these species.

Structure 1: Based on the HSQC spectrum in Fig. 5d, the protons H1 at 3.77 and H2 at 6.06 ppm are seen to be directly attached to the carbon C1 at 70.4 ppm and C2 at 98.2 ppm, respectively. In HMBC spectrum in Fig. 5c, the protons H1 and H2 are seen to have cross peaks to C2 and C1, respectively. The carbon C2 at 98.2 ppm could be assigned the O–C–O unit based on the chemical shift of the carbon. Based on this chemical shift, these signals fit to structure 1 as shown in Scheme 1.

The first step to form this product is the nucleophilic attack on the VC by the hydroxide, leading to ring-opening of VC, which results in vinylene glycol (–O–CH=CH–OH) moiety along with release of CO_2. This moiety can, in turn, trigger polymerization with more VC molecules leading to longer chains of which can further eliminate CO_2, as shown as in route 1 in Scheme 1. A similar product was also claimed by Balbuena and team in their work where they have confirmed through computational calculations that the decarboxylated radical anion of an electrochemically reduced VC molecule indeed could be the starting point for a VC polymerization.[7] There is no direct evidence of the vinylene glycol in our NMR analysis. However, the formation of –CH(OR)$_2$ fragments in our product can plausibly arise when double bonds of the vinylene glycol can themselves undergo hydrolysis reaction (via a simple addition reaction) ultimately leading to specie with structure 1. This proposed chemical reaction could explain the consumption of water during the chemical reaction. Moreover, this specific chemical reaction route satisfies the stoichiometry of 1 VC molecule reacting with ∼1 H_2O molecule obtained from the abovementioned kinetic study.

Table II. ^{1}H and ^{13}C NMR chemical shifts of dissolved solution with DMSO-d_6 of the products formed from VC decomposition.

^{1}H chem. shift (ppm)	^{13}C chem. shift (ppm)	Assignment	Molecular fragments	Corresponding structure
3.77	70.4	1	–CH$_2$O–	Structure 1
6.06	98.2	2	–CH(OR)$_2$–	
4.57, 4.22	69.6	3	–CH$_2$O–	
5.87	100.8	4	–CH(OR)$_2$–	Structure 2
—	154.3	5	–O(C=O)O–	

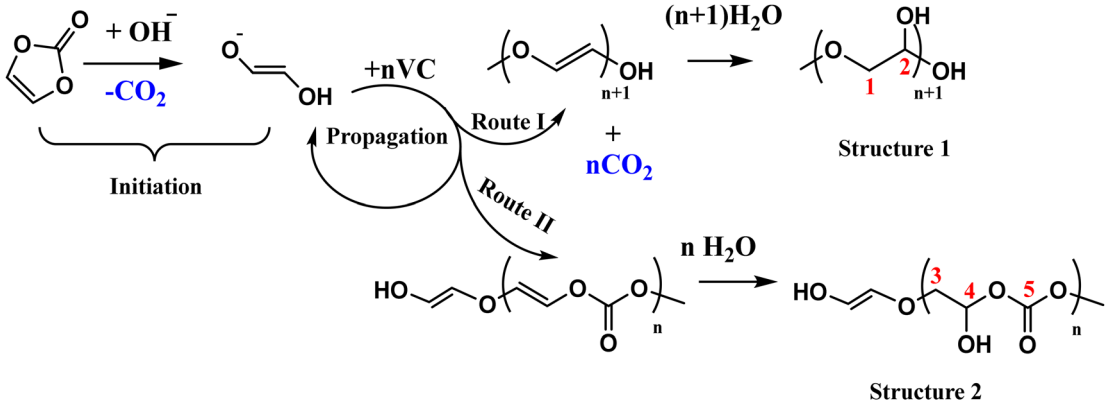

Scheme 1. Proposed scheme for chemical decomposition pathways of VC. The numbers in red in the structures are assigned to the carbons that will be used for their assignment in Table II.

Structure 2: The protons H3 at 4.57 and 4.22 ppm are found to be directly attached to the carbon C3 at 69.6 ppm in the HSQC spectrum in Fig. 5d. The protons H3/H3′ have a multi-bond correlation to the carbon C4 at 100.8 and carbonate carbon C5 at 154.3 ppm, as can be seen in the HMBC spectrum in Fig. 5c. Likewise, the protons H4 at 5.87 ppm have multi-bond correlation to the carbons C3 at 69.6 and carbonate carbon C5 at 154.3. Based on the HSQC spectrum, the proton H4 at 5.87 ppm and H3 at 4.57/4.22 were directly attached to the carbon C4 at 100.8 and C3 at 69.6 ppm, respectively. Based on this chemical shift, species with structure 2 has been determined as shown in Scheme 1. These chemical shifts are in close agreement with the NMR study made by Ota et al., where they reported this compound as one of the SEI compounds derived from VC.[1] We also estimate that structure 2 is a polymer component because the protons H3 and H4 consist of broad peaks. This is largely due to poor molecular rotation and repeating units being situated in marginally different chemical environments resulting into broad signals.

The structure 2 can plausibly form through a route (route 2) where the vinylene glycol moiety undergo polymerization reaction with VC molecules without the evolution of CO_2. This reaction results in formation of polycarbonates. The double bond can again undergo simple addition reaction leading to the structure 2. There is also possibility that these two polymer chains, with structures 1 and 2 as the repeating units, could be part of the same polymer chain.

NMR analyses of the products from the reactions of VC with different amounts of TBAOH.30H_2O show similar mixtures of chemical specie in similar ratios. Additionally, we do not see any evidence of poly(VC) which implies that poly(VC) must be a product of electrochemical reduction of VC and not a product of VC hydrolysis. However, it could also be that poly(VC) is insoluble, hence not detected with solution NMR

Conclusions

Herein, a study of the ring-opening reactions of VC (vinylene carbonate) in presence of water triggered by hydroxide ions is presented. Using injection cell-coupled mass spectrometry, we demonstrate that VC and its saturated counterpart, EC, do not undergo rapid decomposition when in contact with H_2O. However, VC decomposes to produce CO_2 significantly faster than EC, upon contacting H_2O in presence of OH^-.

The subsequent consumption of H_2O by ring-opened reaction products of VC is evidenced for the first time in this study. This was shown by Karl-Fischer titration performed on a background solvent that was deliberately contaminated with water onto which VC was added with and without OH^-. Decomposition of VC produces a mixture of different soluble chain polymers containing oxygenic-groups as detected by solution NMR. The possible reaction pathways resulting in these species involving CO_2 evolution are suggested. It is proposed that the H_2O scavenging capability of VC is due to the double bonds of the linear polymer chains formed from VC ring-opening and polymerisation, which make VC much more susceptible to hydrolysis by simple addition reaction. While the proposed reaction scheme leading to these chemical species is reasonable, it is not conclusive, leaving room for the possibility of additional species forming and resulting in similar chemical signatures. Moreover, it is found that the amount of CO_2 evolved scales with the concentration of VC and is independent of the amount of OH^- (and H_2O) present in the reaction mixture. However, the consumption rate of VC is found to be same as that of H_2O in the reaction, i.e., 1 VC reacts with 1 H_2O molecule.

Although Li-ion cells are assembled in dry rooms, H_2O is notoriously difficult to get rid of and there are always trace amounts of water present. In a cell with VC present as additive, VC would react much faster than EC with H_2O forming largely insoluble species. Hydrolysis of EC and the generation of soluble products, such as ethylene glycol, is therefore suppressed. Ethylene glycol can propagate these side-reactions to a much larger extent and is more harmful to cell performance. The observation that EC continuously evolve CO_2 in presence of H_2O and OH^- while the CO_2 evolution from VC ring-opening rapidly stops despite remaining large amounts of VC supports such a scenario. The lower extent of side-reactions can also explain the much thinner SEI layers present when VC is present, since the decomposition products of EC also eventually will precipitate out of the electrolyte solution when a critical concentration is reached. In conclusion, the commonly observed positive impact of VC on Li-ion cell performance is likely a concerted effect of multiple reaction pathways not explained by a single electrochemical reaction as often previously argued. Further detailed studies of the insoluble products of VC are however necessary to confirm VC reduction product composition and its function in the SEI layer.

Acknowledgments

The authors acknowledge the Knut and Alice Wallenberg (KAW) Foundation (grant 2017.0204), Swedish Research Council (2016–-04069), and Stiftelsen för Strategisk Forskning (SSF, FFL18–0269) for financial support and StandUp for Energy and the national strategic e-Science program eSSENCE for base funding.

ORCID

Neeha Gogoi https://orcid.org/0000-0002-0481-5544
Robin Lundström https://orcid.org/0000-0001-9070-9264
Guiomar Hernández https://orcid.org/0000-0002-2004-5869
Erik J. Berg https://orcid.org/0000-0001-5653-0383

References

1. H. Ota, Y. Sakata, A. Inoue, and S. Yamaguchi, "Analysis of vinylene carbonate derived sei layers on graphite anode." *J. Electrochem. Soc.*, **151**, A1659 (2004).
2. R. Bernhard, M. Metzger, and H. A. Gasteiger, "Gas evolution at graphite anodes depending on electrolyte water content and SEI quality studied by on-line electrochemical mass spectrometry." *J. Electrochem. Soc.*, **162**, A1984 (2015).

3. S. Grugeon, P. Jankowski, D. Cailleu, C. Forestier, L. Sannier, M. Armand, P. Johansson, and S. Laruelle, "Towards a better understanding of vinylene carbonate derived SEI-layers by synthesis of reduction compounds." *J. Power Sources*, **427**, 77 (2019).
4. Y. Wang, S. Nakamura, K. Tasaki, and P. B. Balbuena, "Theoretical studies to understand surface chemistry on carbon anodes for lithium-ion batteries: how does vinylene carbonate play its role as an electrolyte additive?" *J. Am. Chem. Soc.*, **124**, 4408 (2002).
5. Y. Kamikawa, K. Amezawa, and K. Terada, "First-principles study on the mechanical properties of polymers formed by the electrochemical reduction of fluoroethylene carbonate and vinylene carbonate." *J. Phys. Chem. C*, **124**, 19937 (2020).
6. L. El Ouatani, R. Dedryvère, C. Siret, P. Biensan, S. Reynaud, P. Iratçabal, and D. Gonbeau, "The effect of vinylene carbonate additive on surface film formation on both electrodes in li-ion batteries." *J. Electrochem. Soc.*, **156**, A103 (2009).
7. F. A. Soto, Y. Ma, J. M. Martinez De La Hoz, J. M. Seminario, and P. B. Balbuena, "Formation and growth mechanisms of solid-electrolyte interphase layers in rechargeable batteries." *Chem. Mater.*, **27**, 7990 (2015).
8. Y. Wang and P. B. Balbuena, "Associations of lithium Alkyl dicarbonates through O···Li···O interactions." *J. Phys. Chem. A*, **106**, 9582 (2002).
9. B. Zhang, M. Metzger, S. Solchenbach, M. Payne, S. Meini, H. A. Gasteiger, A. Garsuch, and B. L. Lucht, "Role of 1,3-Propane sultone and vinylene carbonate in solid electrolyte interface formation and gas generation." *J. Phys. Chem. C*, **119**, 11337 (2015).
10. P. G. Kitz, M. J. Lacey, P. Novák, and E. J. Berg, "Operando investigation of the solid electrolyte interphase mechanical and transport properties formed from vinylene carbonate and fluoroethylene carbonate." *J. Power Sources*, **477**, 0 (2020).
11. M. Nie, J. Demeaux, B. T. Young, D. R. Heskett, Y. Chen, A. Bose, J. C. Woicik, and B. L. Lucht, "Effect of vinylene carbonate and fluoroethylene carbonate on SEI formation on graphitic anodes in li-ion batteries." *J. Electrochem. Soc.*, **162**, A7008 (2015).
12. X. Zhang, R. Kostecki, T. J. Richardson, J. K. Pugh, and P. N. Ross, "Electrochemical and infrared studies of the reduction of organic carbonates." *J. Electrochem. Soc.*, **148**, A1341 (2001).
13. K. U. Schwenke, S. Solchenbach, J. Demeaux, B. L. Lucht, and H. A. Gasteiger, "The impact of CO 2 evolved from VC and FEC during formation of graphite anodes in lithium-ion batteries." *J. Electrochem. Soc.*, **166**, A2035 (2019).
14. M. Metzger, B. Strehle, S. Solchenbach, and H. A. Gasteiger, "Hydrolysis of ethylene carbonate with water and hydroxide under battery operating conditions." *J. Electrochem. Soc.*, **163**, A1219 (2016).
15. R. Lundström and E. J. Berg, "Design and validation of an online partial and total pressure measurement system for li-ion cells." *J. Power Sources*, **485**, 229347 (2021).
16. M. Tang, S. Lu, and J. Newman, "Experimental and theoretical investigation of solid-electrolyte-interphase formation mechanisms on glassy carbon." *J. Electrochem. Soc.*, **159**, A1775 (2012).
17. B. Scrosati and Y. Sun, "Influence of temperature on lithium − oxygen battery behavior." *Nano Lett.*, **13**, 2971 (2013).
18. R. Petibon, J. Xia, J. C. Burns, and J. R. Dahn, "Study of the consumption of vinylene carbonate in Li[Ni 0.33 Mn 0.33 Co 0.33]O2/graphite pouch cells." *J. Electrochem. Soc.*, **161**, A1618 (2014).